[1] Institute of Tibetan Plateau Research, Chinese Academy of Sciences, Beijing, China
[2] Cold and Arid Regions Environmental and Engineering Research Institute,
Chinese Academy of Sciences, Lanzhou, China
[3] College of Life Science and Technique, Shanxi University, Taiyuan, China
[4] Disaster Prevention Research Institute, Kyoto University, Japan
[5] Department of Earth Sciences, Okayama University, Okayama, Japan
[6] Department of Civil Engineering, University of Tokyo, Japan
[7] Alterra Green World Research, Wageningen University and Research Centre, The Netherlands

Diurnal and inter-monthly variation of land surface heat fluxes over the central Tibetan Plateau area

Y. Ma[1,2]**, S. Fan**[3]**, H. Ishikawa**[4]**, O. Tsukamoto**[5]**, T. Yao**[1,2]**, T. Koike**[6]**,
H. Zuo**[1]**, Z. Hu**[1]**,** and **Z. Su**[7]

With 7 Figures

Summary

The energy and water cycle over the Tibetan Plateau play an important role in the Asian monsoon system, which in turn is a major component of both the energy and water cycles of the global climate system. Using field observational data observed from the GAME/Tibet (GEWEX (Global Energy and Water cycle Experiment) Asian Monsoon Experiment on the Tibetan Plateau) and the CAMP/Tibet (CEOP (Coordinated Enhanced Observing Period) Asia-Australia Monsoon Project (CAMP) on the Tibetan Plateau), some results on the local surface energy partitioning (diurnal variation, inter-monthly variation and vertical variation etc.) are presented in this study.

The study on the regional surface energy partitioning is of paramount importance over heterogeneous landscape of the Tibetan Plateau and it is also one of the main scientific objectives of the GAME/Tibet and the CAMP/Tibet. Therefore, the regional distributions and their inter-monthly variations of surface heat fluxes (net radiation flux, soil heat flux, sensible heat flux and latent heat flux) are also derived by combining NOAA-14/AVHRR data with field observations. The derived results were validated by using the "ground truth", and it shows that the derived regional distributions and their inter-monthly variations of land surface heat fluxes are reasonable by using the method proposed in this study. Further improvement of the method and its applying field were also discussed.

1. Introduction

As the most prominent and complicated terrain on the globe, the Tibetan Plateau (Ye and Gao, 1979; Ye, 1981; Ye and Wu, 1998; Yanai et al., 1992), with an elevation of more than 4000 m on average above mean sea leave (*msl*) makes up approximately one fourth of the land area of China. Long-term research on the Tibetan Plateau have shown that the giant prominence exerts thermal effects on the atmosphere, thus greatly influencing circulations over China, Asia and even the globe (Ye and Gao, 1979; Ye, 1981; Ye and Wu, 1998; Yanai et al., 1992; Ma et al., 2002a; Ma and Tsukamoto, 2002b). Due to its topographic character, the plateau surface absorbs a large amount of solar radiation energy (much of which is redistributed by cryospheric processes), and undergoes dramatic seasonal changes of surface heat and water

fluxes (Ye and Gao, 1979; Ye and Wu, 1998; Yanai et al., 1992). The lack of quantitative understanding of interactions between the land surface and atmosphere makes it difficult to understand the complete energy and water cycles over the Tibetan Plateau and their effects on the Asian monsoon system with numerical models. Therefore, it has increased the number of land surface processes studies over the Tibetan Plateau in the past 30 years. But the previous experiments were only carried out in a short period and the observational items were limited, and the previous investigations were only in summer period and on some points or local level (Zhang et al., 1988; Ye and Wu, 1998; Ma et al., 2002a; Ma and Tsukamoto, 2002b).

The intensive observation period (IOP) and long-term observation of the GAME/Tibet (GEWEX (Global Energy and Water cycle Experiment) Asian Monsoon Experiment on the Tibetan Plateau, 1996–2000) and the CAMP/Tibet (CEOP (Coordinated Enhanced Observing Period) Asia–Australia Monsoon Project (CAMP) on the Tibetan Plateau, 2001–2005) have been done successfully in the past 7 years. A large amount of data has been collected, which is the best data set so far for the study of energy and water cycle over the Tibetan Plateau. It gives us a chance to investigate the energy and water cycle over the Tibetan Plateau in detail.

The purpose of this study is to analyze the characteristics of local and regional surface energy partitioning by using the field observational data and NOAA-14/AVHRR data collected during the GAME/Tibet and the CAMP/Tibet.

2. Experiment

The field experiments of GAME/Tibet and CAMP/Tibet will be introduced in this section.

2.1 Experiment of the GAME/Tibet

The overall goal of the GAME/Tibet is to clarify the interaction between the land surface and the atmosphere over the Tibetan Plateau in the context of the Asian monsoon system. To achieve this goal, the scientific objectives of the GAME/Tibet are to improve the quantitative understanding of land-atmosphere interactions over the Tibetan Plateau, to develop process models and methods for applying them over large spatial scales, and to develop and validate satellite-based retrieval methods. The GAME/Tibet is an inter-disciplinary, coordinated effort by filed scientists, modelers and remote sensing scientists in meteorology and hydrology to address these objectives.

Figure 1a is the sites layout during IOP of the GAME/Tibet. A meso-scale observational network (150 × 250 km, 91°–92.5° E, 30.5°–33° N) was implemented in the central plateau: (1) Anduo PBL station (91° 37′30″E, 32° 14′28″N, elevation: 4700 m). A PBL tower (17 m, wind speed, wind direction, air temperature and humidity at three-levels), radiation observational system, the turbulent flux measurements (sonic anemo-thermometer), soil temperature and moisture measurement, radio sonde observation system etc. have been set up in this station; (2) AWS networks. Five AWS (Automatic Weather Station, D66, TTH, Naqu, D110, MS3608) and two sets of flux-PAM (Portable Automated Meso-net, MS3478-NPAM and MS3637-SPAM) stations have been deployed along the Tibetan (Qinghai-Xizang) high way; (3) A basic PBL observational station (NaquFx). A PBL tower (3.5 m, four-levels), radiation observational system, the turbulent flux measurements (sonic anemo-thermometer), soil temperature, moisture measurement and soil water content have been set up in this station in 1998; (4) Barometer network (nine sites: Anduo, AQB, Naqu, Noda, North-mt, South-mt, Sexi, Ziri, Wadd), the ground truth observation sites for validation of satellite data, the sampling network for isotope study on water cycle; (5) Soil temperature and soil moisture network (SMTMS). Nine SMTMS sites (D66, TTH, D110, WADD, NODA, Anduo, MS3478, MS3608 and MS3637) have been deployed along the Tibetan high way; (6) Three-dimensional Doppler radar and precipitation gauge network. The Doppler radar system has been deployed about 10 km south of Naqu in 1998 (91° 56′20″E, 31° 22′59″N). Seven rain gauges were set up around the radar station; (7) Precipitation gauge net (D110, WADD, NODA, AQB, MS3478, MS3543, Zuri, NaquFx, MS3608, Naquhy, NaquRS and MS3637) has been deployed along the Tibetan high way; and (8) two radio-sonde observational systems were set up in Anduo PBL station and Naqu Meteorological Bureau.
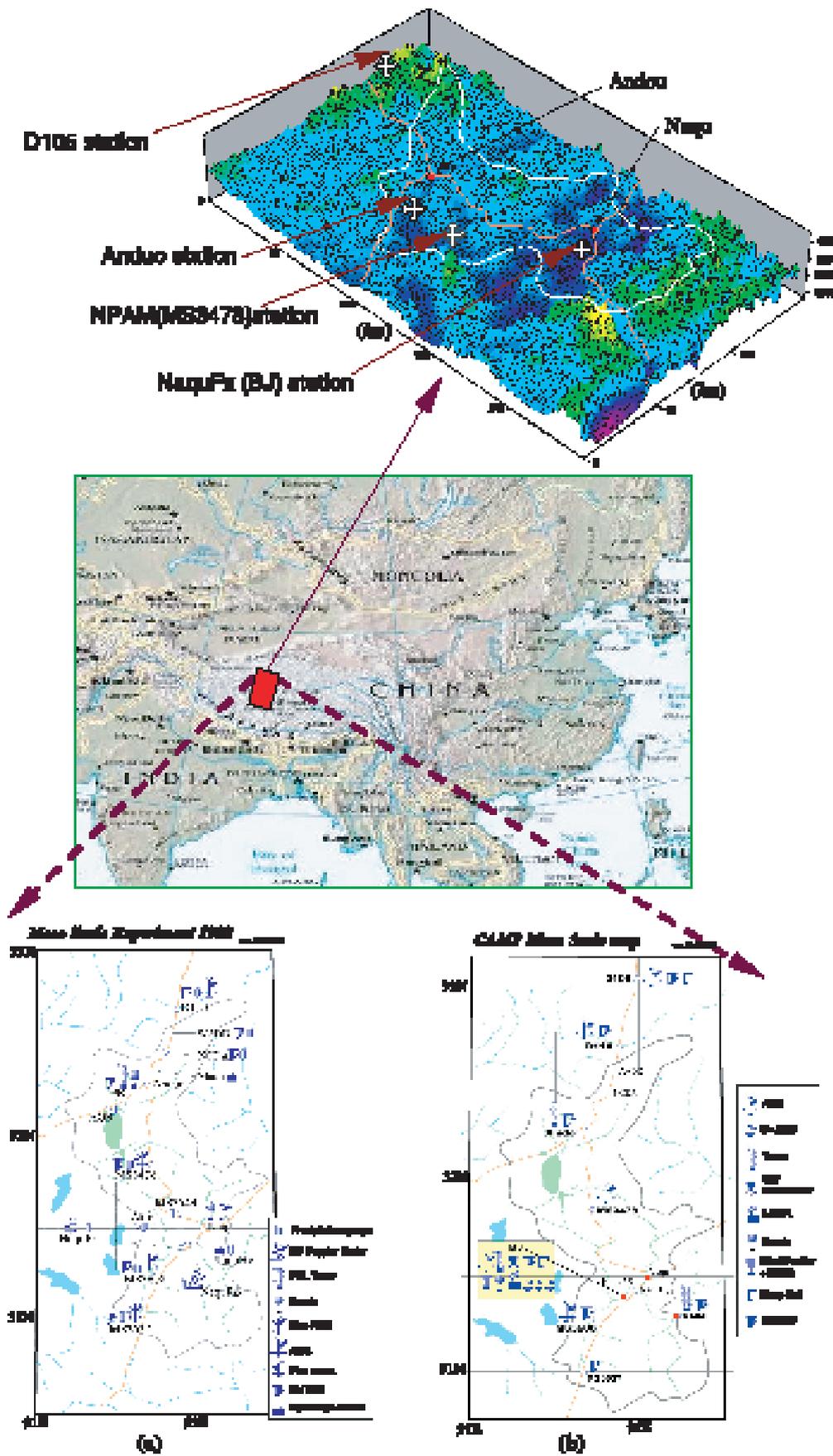
Fig. 1. The geographic map and the sites layout during the GAME/Tibet and the CAMP/Tibet

The IOP of GAME/Tibet has been done successfully during May through September 1998.

2.2 Experiment of the CAMP/Tibet

The objectives of CAMP/Tibet are: 1) Quantitative understanding of an entire seasonal hydrometeorological cycle including winter processes by solving surface energy "imbalance" problems in the Tibetan Plateau; 2) Observation of local circulation and evaluation of its impact on plateau scale water and energy cycle; and 3) Establishment of quantitative observational methods for entire water and energy cycle between land surface and atmosphere by using satellites. To achieve the scientific objectives of CAMP/Tibet, a meso-scale observational network (150×250 km, $91°$–$92.5°$ E, $30.7°$–$33.3°$ N) were implemented in the central plateau (Fig. 1b): 1) A basic observational station (BJ). A flux measuring tower (20 m, two levels), a Sky Radiometer, a LIDAR system, a Wind Profiler and RASS, a radio sonde system, and 4 AWSs have been set up at this station; (2) AWS networks. Six AWS (D105, D110, MS3478, BJ, MS3608 and ANNI) stations have been deployed in this area; (3) Soil moisture and soil temperature (SMTMS) networks. Seven SMTMS sites (D105, D110, Anduo, BJ, MS3608, ANNI and MS3637) have been deployed in this area; (4) Two deep soil temperature measurements were put in D105 and NaquDS (nearby the BJ basic station); (5) Anduo PBL station ($91° 37'30''$E, $32° 14'28''$N). A PBL tower (17 m, wind speed, wind direction, air temperature and humidity at three-levels) and radiation observational system have already been continued for 6 years from 1997 and will be continued for another two years till the end of 2005. The enhanced automated observing period (EAOP) and IOP of the CAMP/Tibet have been started from October 1, 2002 and will be continued to September 30, 2004.

3. Data analysis and results

3.1 Diurnal and inter-monthly variation of local land surface heat fluxes

The field data observed at three AWS stations (D105, BJ and MS3478) of the CAMP/Tibet under the clear day will be used in this section.

The reason is that each component of surface radiation budget (downward short wave and long wave radiation and upward short wave and long wave radiation) and land surface heat flux budget (net radiation flux, soil heat flux, sensible heat flux and latent heat flux) will be in truth-value under the condition of clear day, and fortunately, there is one clear day each month at least during the measurement period. The geographical coordinates of three AWS stations are, D105: ($91° 54'22''$E, $33° 4'2''$N), BJ: ($91° 48'59''$E, $31° 18'42''$N) and MS3478-NPAM: ($91° 42'10''$E, $31° 54'15''$N). The elevations of three AWS stations are, D105: 5020 m, BJ: 4580 m and MS3478-NPAM: 5063 m. The selected data period is from September 2000 to August 2001.

3.1.1 Local radiation energy budget

Figure 2 gives the diurnal variation and inter-monthly variation curves of each component of surface radiation budget in the stations (D105, BJ and MS3478) of the CAMP/Tibet, including downward short wave radiation (SD), downward long wave radiation (LD), upward long wave radiation (LU) and upward short wave radiation (SU). One clear day data was selected in each month, and the point of the diurnal cycle for one month stops and the next month starts was just at the center of between two days curves in Fig. 2. It can be seen that: 1) The inter-monthly variation of the downward short wave radiation was very obvious. The summer values were larger than those in winter, and it reach the minimum value around December. Although the downward long wave radiation, the upward long wave radiation and upward short wave radiation had different values in different months, their inter-monthly variations were not clear; 2) The diurnal variations of downward short wave radiation, upward short wave radiation and upward long wave radiation were very obvious, and the diurnal variation of downward long wave radiation was not clear. It means that when the sun rises at around 0800 BT (Beijing Time) in the morning, they increase with the increasing of solar altitude angle, and the maximum value appears at about 1300 BT, then they decrease with the decreasing of solar altitude angle. Downward and upward short wave radiations become zero and negative at about 2000 BT in
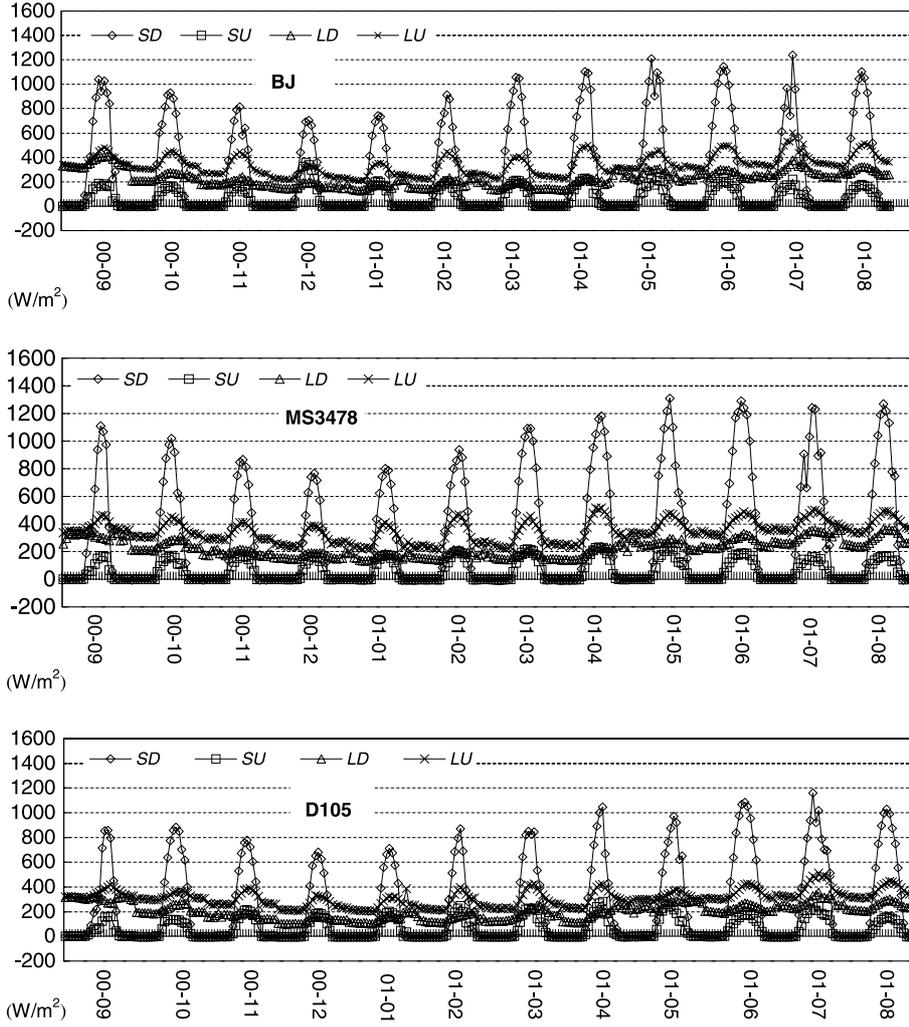
Fig. 2. The inter-monthly variations of radiation fluxes in the Tibetan Plateau area

the nightfall; 3) The downward short wave radiation (*SD*) reaches about $1200\,\text{W}/\text{m}^2$ or more at local noon on fine days in summer. The transmission rate of incoming solar radiation from the top of the atmosphere was estimated as about 85% in cloudless conditions. The values are about 10–15% great than those observed at the typical sea level station. It is due to the high altitude of the site, thus a shallower atmospheric layer between the top of the atmospheric and the ground surface.

3.1.2 Local land surface energy budget

Using data observed at three AWS stations (D105, BJ and MS3478) of the CAMP/Tibet, the turbulent fluxes will be determined as

sensible heat flux $H = \rho C_p C_{HN}(u_z - u_s)$
$$\cdot (T_{sfc} - T_z), \qquad (1)$$

latent heat flux $LE = \rho L C_{EN}(u_z - u_s)(q_{sfc} - q_z)$
$$= H \cdot B^{-1}, \qquad (2)$$

$$\text{Bowen ratio } B = \frac{H}{LE} = \frac{C_p(T_{z_1} - T_{z_2})}{L(q_{z_1} - q_{z_2})}, \qquad (3)$$

where ρ is air density, C_p is air specific heat at constant pressure, L is latent heat of vaporization, E is evaporation flux, u_z, T_z and q_z are wind speed, air temperature and specific humidity at the height z; u_s, T_{sfc} and q_{sfc} are wind speed, air temperature and specific humidity on the land surface; C_{HN} and C_{EN} are the bulk transfer coefficients in the neutral state. Normally, C_{HN} and C_{EN} are taken to be identical in the neutral state, and

$$C_{HN} = \frac{k^2}{[\ln(z/z_{0m})]^2}, \qquad (4)$$

where k is von Karman constant, and z_{om} is aerodynamic roughness length. z_{om} over the Tibetan Plateau area can be determined by using the turbulence data observed with a sonic anemometer–

thermometer, PBL tower data and AWS data (Ma et al., 2002a; Ma and Tsukamoto, 2002b).

Figure 3 shows the diurnal variations and inter-monthly variations of surface heat fluxes at the
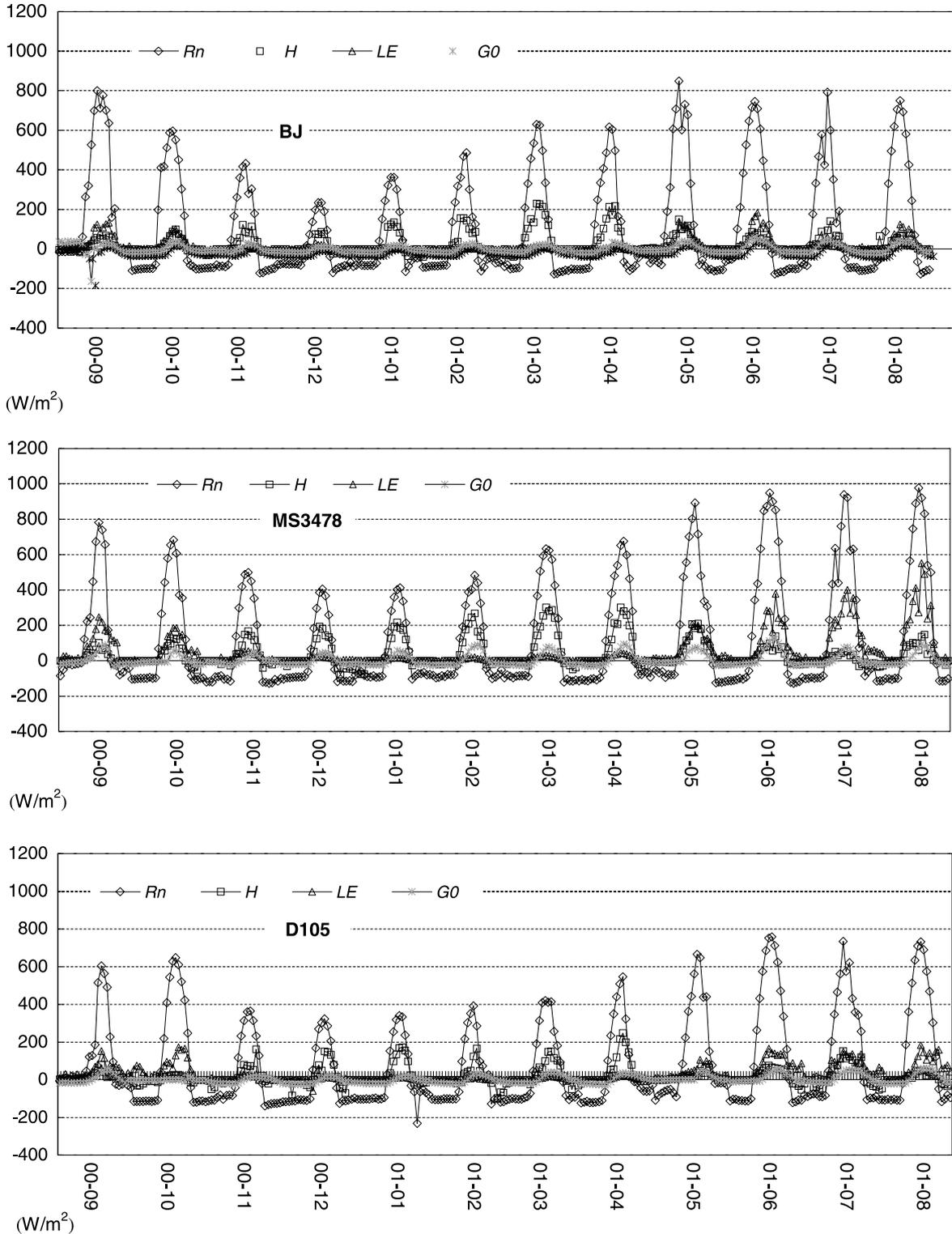

Fig. 3. The diurnal variation and inter-monthly variation of land surface heat fluxes at the CAMP/Tibet stations

stations (D105, BJ, and MS3478) of the CAMP/Tibet, including net radiation flux (R_n), sensible heat flux (H), latent heat flux (LE) and soil heat flux (G_0). One clear day data was selected in each month, and the point of the diurnal cycle for one month stops and the diurnal cycle for the next month starts was just at the center of between two days curves in Fig. 3. The results show that: 1) The diurnal variations for surface heat fluxes in the Tibetan Plateau area are very clear. Net radiation flux in each month at MS3478 station is larger than that at D105 station and BJ station due to the good vegetation coverage at this station (lower up-ward long wave radiation); 2) Sensible heat and latent heat fluxes play different roles in the partition of net radiation flux in different month in the Tibetan Plateau. In other words, sensible heat flux plays the main role in winter and latent heat flux plays the main role in summer and autumn; 3) The surface energy budget was, however, not well closed from the observed data. $CR = (H + LE)/(R_n - G_0)$, the present results show $CR = 0.7$ and sometimes as low as 0.67. This kind of "imbalances" was also found not only from PBL data analysis, but also from sonic-anemometer data analysis (Ma et al., 2000; Tanaka et al., 2001). And the "imbalance" is larger in summer than in winter. There are various possibilities for this "imbalance": a) measurement problems (Ma et al., 2000); b) advections around the experimental stations (Ma et al., 2000); c) there exist a discussion that a very weak systematic vertical flow can cause such an imbalance (Lee, 1998).

3.2 Vertical variation of local surface heat fluxes

Turbulence data observed with two sonic anemometer–thermometer (Kaijo-Denki DAT-300, path 20 cm) and two LICOR-7500 hygrometer (LI-COR, inc.) on two levels (3 m and 20 m) at BJ station of the CAMP/Tibet was processed using the eddy correlation methodology. Some main calculation equations are

Sensible heat flux: $H = \rho C_P \overline{w'T'}$
$$= -\rho C_P u_* T_*, \qquad (5)$$

Latent heat flux: $LE = L\rho \overline{w'q'}$
$$= -L\rho u_* q_*, \qquad (6)$$

Friction velocity: $u_* = \sqrt{|-\overline{u'w'}|}, \qquad (7)$

Characteristic temperature: $T_* = -\dfrac{\overline{w'T'}}{u_*}, \qquad (8)$

Characteristic specific humidity: $q_* = -\dfrac{\overline{w'q'}}{u_*},$
$$\qquad (9)$$

Stability parameter: $\zeta = -\dfrac{zTu_*{}^3}{kg\overline{w'T'}}$
$$= -\dfrac{zTu_*{}^3 \rho C_P}{kgH}. \qquad (10)$$

where u', w', T', q' are the fluctuation of horizontal wind speed, vertical wind speed, air temperature and specific humidity, T is air temperature, and g is gravitational acceleration.

Figure 4 shows the diurnal variations of sensible heat flux and latent heat flux on two levels (3 m and 20 m) in Jun. 24 and Aug. 24, 2002 at BJ station. The results show that the fluxes vary by less than 10% of their magnitude with the height over the Tibetan Plateau area. It means that surface layer over the Tibetan Plateau is a constant flux layer. Therefore, Monin-Obukhov similarity can be used to this area.

3.3 The distribution and inter-monthly variation of regional land surface heat fluxes

The study on the regional surface energy partitioning and its inter-monthly variation is of paramount importance over heterogeneous landscape of the Tibetan Plateau and it is also one of the main scientific objectives of the GAME/Tibet and the CAMP/Tibet. Therefore, we will try to derive the regional land surface heat fluxes by using the NOAA-14/AVHRR data and the field observational data here. Here, "Regional" land surface heat fluxes are not "aggregated" fluxes (Batchvarova et al., 2001), but surface fluxes fields or surface heat fluxes on each pixel of NOAA-14/AVHRR data.

The general concept of the methodology is shown in a diagram (Fig. 5). The surface reflectance for short-wave radiation (r_0), land surface temperature (T_{sfc}), are retrieved from NOAA-14/AVHRR data with the atmospheric correction by using radiative transfer model MODTRAN
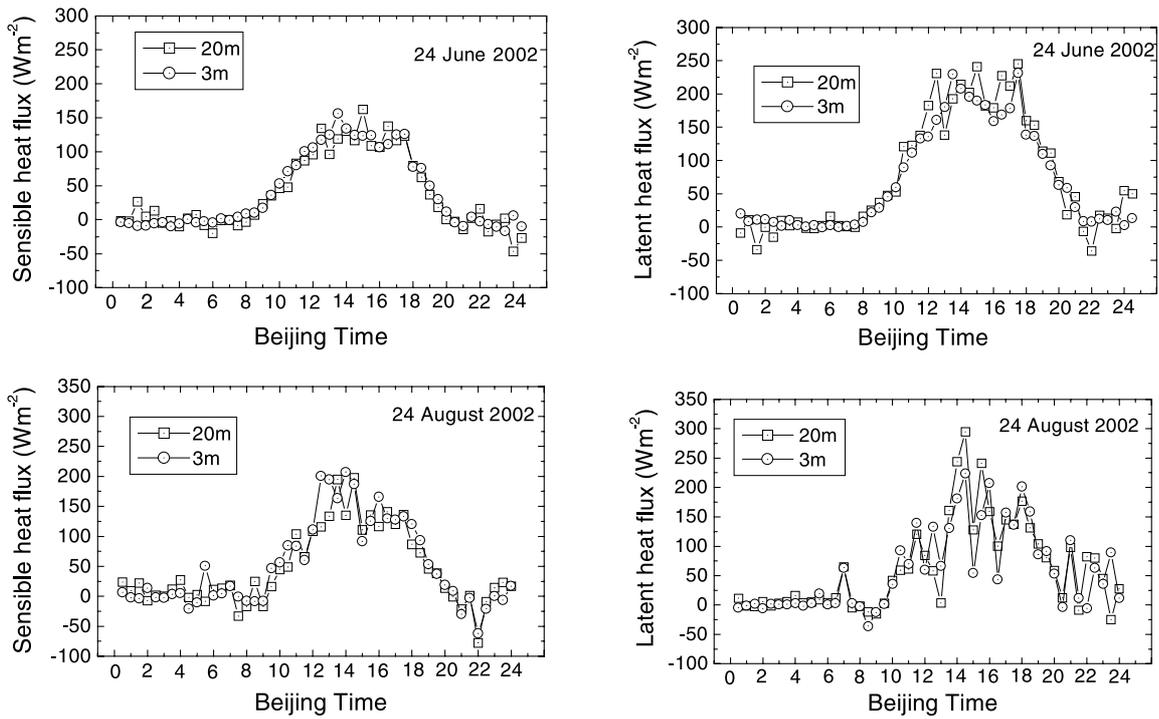
Fig. 4. The diurnal variations of sensible heat fluxes and latent heat flux on two levels (3 m and 20 m) in Jun. 24 and Aug. 24, 2002 at BJ station of the CAMP/Tibet
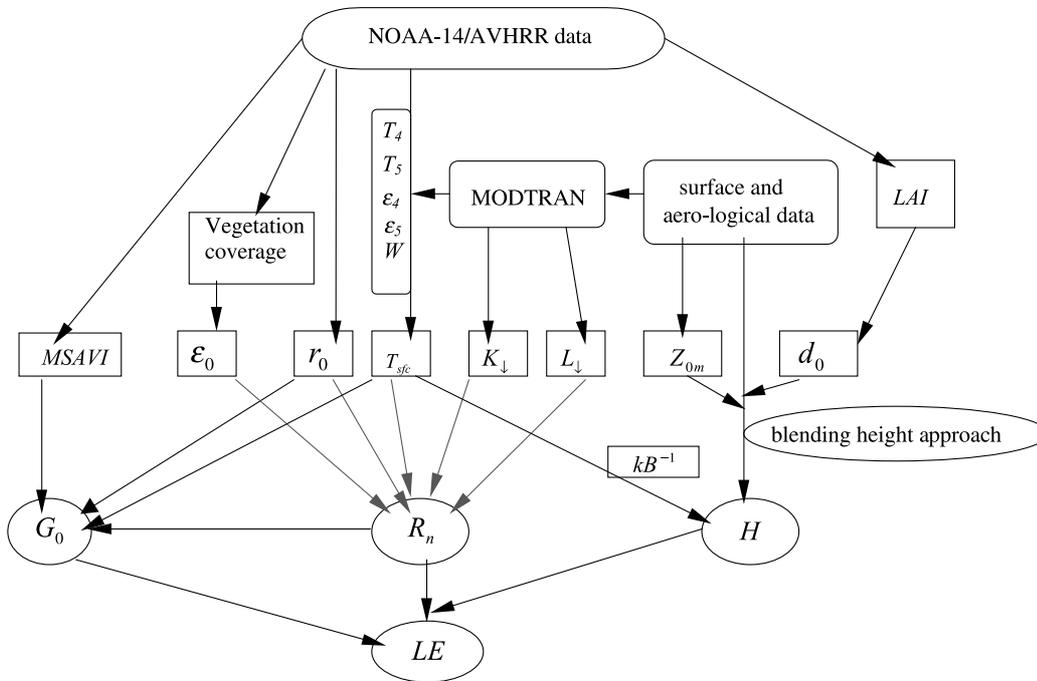

Fig. 5. Diagram of parameterization procedure combining NOAA-14/AVHRR data with field observations

(Berk et al., 1989) and aero logical observational data. The radiative transfer model also computes the downward short- and long-wave radiation at the surface. With these results the surface net radiation (R_n) is determined. The soil heat flux (G_0) is estimated from R_n, T_{sfc}, r_0 and *MSAVI*

(Modified Soil Adjusted Vegetation Index, Qi et al., 1994) which is also derived from NOAA-14/AVHRR data. Sensible heat flux (H) is estimated from T_{sfc}, surface and aero logical data with the aid of so called 'blending height' approach (Mason, 1988).

3.3.1 Net radiation

The regional net radiation flux is expressed as
$$R_n(x,y) = (1 - r_0(x,y)) \cdot K_\downarrow(x,y) + L_\downarrow(x,y)$$
$$- \varepsilon_0(x,y)\sigma T_{sfc}{}^4(x,y), \qquad (11)$$
where σ is Stefan Boltzmann constant and surface reflectance $r_0(x,y)$ is derived from the channel-1 and -2 of NOAA-14/AVHRR data with the models of Paltridge and Mitchell (1990) and Valiente et al. (1995). Surface reflectance of each pixel $r_0(x,y)$ should be considered as an effective reflectance, it is not only a function of the surface coverage but also of the solar elevation angle (Gryning et al., 2001). The surface emissivity $\varepsilon_0(x,y)$ is a function of the vegetation coverage, and is also derived from channel 1 and 2 data with the algorithm by Valor and Caselles (1996). The incoming short-wave radiation flux $K_\downarrow(x,y)$ and the incoming long-wave radiation flux $L_\downarrow(x,y)$ in Eq. (11) can be derived from radiative transfer model MODTRAN (Kneizys et al., 1996) directly. The land surface temperature $T_{sfc}(x,y)$ is retrieved from the brightness temperature of channels four and five of NOAA-14/AVHRR according to Sobrino and Raissouni (2000) in this study, i.e.
$$T_{sfc}(x,y) = T_4(x,y) + 1.40[T_4(x,y) - T_5(x,y)]$$
$$+ 0.28[T_4(x,y) - T_5(x,y)]^2$$
$$+ 0.83 + (57 - 5W)(1 - \varepsilon)$$
$$- (161 - 30W)\Delta\varepsilon \qquad (12)$$
where $\varepsilon = (\varepsilon_4 + \varepsilon_5)/2$, $\Delta\varepsilon = \varepsilon_4 - \varepsilon_5$ (Li and Becker, 1993), ε_4 and ε_5 are spectral emissivity of channel 4 and channel 5 of NOAA/AVHRR, T_4 and T_5 are brightness temperature of channel 4 and channel 5 of NOAA/AVHRR, W is water vapor content.

3.3.2 Soil heat flux

The regional soil heat flux $G_0(x,y)$ is usually determined by (Choudhury and Monteith, 1988)
$$G_0(x,y) = \rho_s C_s[(T_{sfc}(x,y) - T_s(x,y)]/r_{sh}(x,y), \qquad (13)$$
where ρ_s is soil dry bulk density, C_s is soil specific heat, $T_s(x,y)$ stands for soil temperature of a determined depth, $r_{sh}(x,y)$ represents soil heat transportation resistance. However, the regional soil heat flux $G_0(x,y)$ cannot directly be mapped from satellite observations through Eq. (13) for the difficulty to determine the soil heat transportation resistance $r_{sh}(x,y)$ and the soil temperature at a reference depth $T_s(x,y)$. Many investigations have shown that the mid-day G_0/R_n fraction is reasonably predicted from special vegetation indices (Daughtry et al., 1990). Some researchers have shown that $G_0/R_n = \Gamma(NDVI)$ (Clothier et al., 1986; Choudhury et al., 1987; Kustas and Daughtry, 1990). An improved fraction of $G_0/R_n = \Gamma(r_0, T_{sfc}, NDVI)$ was proposed (Menenti et al., 1991; Bastiaanssen, 1995). However, problems exist in the $NDVI$ definition equation because of the effects of external factors, such as soil background variations (Huete et al., 1985; Huete, 1989). In order to reduce the soil background effect in $NDVI$, a parameterization based on $MSAVI$ is proposed over the Tibetan area in this study as
$$G_0(x,y) = R_n(x,y) \cdot (T_{sfc}(x,y)/r_0(x,y))$$
$$\cdot (a + b\bar{r}_0 + c\bar{r}_0{}^2)$$
$$\cdot [1 + dMSAVI(x,y)^e], \qquad (14)$$
where the constants a, b, c, d and e are determined by using the field data observed at six observation stations (AWS110, Anduo, NPAM-MS3478, Naqu, AWS3608 and SPAM-MS3637) during the GAME/Tibet IOP; $\overline{r_0}$ is a daily mean reflectance value obtained from field observations. $MSAVI$ (x,y) is derived from the band reflectance of channel 1 and 2 of NOAA-14/AVHRR as (Qi et al., 1994)

$$MSAVI(x,y) = \frac{2r_2(x,y) + 1 - \sqrt{[2r_2(x,y) + 1]^2 - 8[r_2(x,y) - r_1(x,y)]}}{2}, \qquad (15)$$

where r_1 and r_2 are the band reflectance of NOAA-14/AVHRR band-1 and band-2 on the land surface.

3.3.3 Sensible and latent heat fluxes

The sensible heat flux $H(x, y)$ can be derived from

mined by using field measurements or numerical models. In this study, these variables will be determined with the aid of radiosonde measurements. $Z_{0m}(x, y)$ is effective aerodynamic roughness length including the effect of topography and low vegetation (e.g. grass), and is determined

$$H(x, y) = \rho C_P k^2 u(x, y) \frac{[T_{sfc}(x, y) - T_a(x, y)]}{\left[\ln \frac{z - d_0(x,y)}{Z_{0m}(x,y)} + kB^{-1}(x, y) - \psi_h(x, y) \right] \cdot \left[\ln \frac{z - d_0(x,y)}{Z_{0m}(x,y)} - \psi_m(x, y) \right]}. \tag{16}$$

The straightforward way to model sensible heat flux in a large area is to sum up the contribution from different surface elements. If the local scale advection is comparatively small, it is desired that the development of convective boundary layer may smooth the local heterogeneity of surface disorganized variety at so called 'blending height', where atmospheric characteristics become approximately independent of horizontal locations. The corresponding 'effective' surface variables can be determined accordingly (Mason, 1988). This approach has been proved to be successful to calculate regional averaged surface fluxes recently (Lhomme et al., 1994; Bastiaassen, 1995; Wang et al., 1995; Ma et al., 1999a; Batchvarova et al., 2001; Ma et al., 2002c). Based on this approach, the regional sensible heat flux $H(x, y)$ is expressed as

by the Taylor's model (Taylor et al., 1989). In other words, local aerodynamic roughness length can be determined by using the observed turbulent data (Chen et al., 1993; Ma et al., 2002a), and Table 1 is local aerodynamic roughness length at two stations (Anduo and NPAM-MS3478) derived from turbulent data (in order to compare each other, local aerodynamic roughness length on other land surface are also given here). Then, effective aerodynamic roughness length $Z_{0m}(x, y)$ can be derived by considering the effect of grass and mountains (Taylor et al., 1989). The excess resistance to heat transfer, kB^{-1}, is shown as a function of surface temperature over Tibetan Plateau area (Ma et al., 2002a). d_0 is zero-plane displacement length, which can be calculated from Raupach's model (Raupach, 1994) over this area. $\psi_h(x, y)$ and $\psi_m(x, y)$ are the

$$H(x, y) = \rho C_P k^2 u_B \frac{[T_{sfc}(x, y) - T_{\text{air-}B}]}{\left[\ln \frac{z_B - d_0(x,y)}{Z_{0m}(x,y)} + kB^{-1}(x, y) - \psi_h(x, y) \right] \cdot \left[\ln \frac{z_B - d_0(x,y)}{Z_{0m}(x,y)} - \psi_m(x, y) \right]}, \tag{17}$$

where Z_B is blending height, u_B and $T_{\text{air-}B}$ are wind speed and air temperature at the blending height respectively. Z_B, u_B and $T_{\text{air-}B}$ are determined

integrated stability functions in Eq. (17). They can be derived by using the models of Paulson (1970) and Webb (1970).

Table 1. Aerodynamic roughness length z_{0m} on different land surface

	Anduo	NPAM	HEIFE desert	HEIFE Gobi	HEIFE oasis	HEIFE oasis	AECMP'95 oasis
Land surface Characteristics	grass land, ~ 5 cm	grass land, ~ 15 cm	sand desert	very sparse vegetation	bean, ~ 0.4 m	wheat, ~ 1.0 m	corn, ~ 1.8 m
Observational Height/m	2.90	5.60	2.90	2.90	2.90	2.90	4.90
z_{0m}/m	0.00436 ± 0.00040	0.00564 (May) 0.0139 (July) 0.0324 (August)	0.00267 ± 0.0003	0.00280 ± 0.00030	0.06100 ± 0.00400	0.16800 ± 0.03000	0.30200 ± 0.0200

The regional latent heat flux $LE(x, y)$ is the residual of the energy budget theorem for land surface, i.e.

$$LE(x, y) = R_n(x, y) - H(x, y) - G_0(x, y). \quad (18)$$

3.3.4 Results

It is better to select the satellite data in clear days to study the distribution and inter-monthly variation of energy budget components. Unfortunately, it is difficult to select this kind of satellite data over the Tibetan Plateau area because of the strong convective clouds when NOAA-14/AVHRR observation took place (around local time 1400). Only three scenes of the NOAA-14/AVHRR could be selected during the whole IOP of the GAME/Tibet. The scene of June 12, 1998 was selected as a case of pre-monsoon and whole meso-scale area. The scenes of July 16, 1998 and August 21, 1998 were selected as the cases of mid-monsoon and the post-monsoon. The images around Anduo station and NPAM station were selected as the comparable areas because fluxes measurements using sonic anemometer-thermometer were undertook at these two stations. It is also very clear around these two stations on the images of NOAA-14/AVHRR.

Figure 6 shows the distribution maps of land surface heat fluxes around Anduo station and NPAM-MS3478 station in different months. It is based on 45 by 40 pixels with a size of $1\,\mathrm{km} \times 1\,\mathrm{km}^2$. The land surface heat fluxes derived from satellite data were compared with the field measurements at Anduo and NPAM-MS3478 sites. They are shown in Fig. 7. The field observational data, which used for validation here, was just measured at the time of satellite over passed the area or ten minutes averaging value around that time. The mean absolute percent difference (MAPD) was computed as a quantitative measure of the difference between the derived results on No. i point ($H_{\mathrm{derived}(i)}$) and measured value on No. i point ($H_{\mathrm{measured}(i)}$) of one scene as,

$$\mathrm{MAPD} = \frac{100}{n} \sum_{i=1}^{n} \left(\frac{|H_{\mathrm{derived}(i)} - H_{\mathrm{measured}(i)}|}{H_{\mathrm{measured}(i)}} \right).$$

$$(19)$$

It is seen that: (1) the derived land surface heat fluxes were in good accordance with the land surface status. These parameters show a wide range of variations due to the strong contrast of surface features in the study area; (2) not only on June 12, but also on July 16 and August 21, the derived net radiation flux, soil heat flux and sensible heat flux were close to the field measurements. The difference between the derived results and the field observation MAPD was less than 10%; (3) during the experimental periods, the derived net radiation flux was larger than that in the HEIFE area (Ma et al., 2002b) due to the high altitude (the higher value of downward short-wave radiation) and land surface coverage of grassy marshland (the lower value of the upward long-wave radiation) in this area. For example, the regional average value of net radiation flux was $470\,\mathrm{W/m}^2$ over the HEIFE area in 9 July, 1991 and that was $750\,\mathrm{W/m}^2$ over the GAME/Tibet area in 16 July, 1998; (4) the values of soil heat flux and sensible heat flux in June over this area were larger than these values in July and August. Net radiation flux and latent heat flux in June were lower than their values in July and August. The reason is that although land surface in this area is covered by the same grassy marshland in these days, June 12 was the day before the Asian monsoon coming, and the land surface was dry in that day, July 16 and August 21 were within and after Asia monsoon, the land surface was wet and the grass was high and in growing; (5) The derived regional soil heat fluxes based on *MSAVI* were reasonable in different months in this area with MAPD less than 10%; and (6) all elements of heat balance equation at NPAM site on June 12 well corresponded to the satellite data. On the other hand, all but latent heat flux corresponded to the satellite data in other seasons and other stations. The conclusions derived from above facts were, (a) net radiation, sensible heat flux and soil heat flux could be derived from satellite, (b) in the case of NPAM on June 12, because the surface energy balanced in the surface observation so that the latent heat flux estimated by surface observation well corresponded to that estimated by the residual of satellite data analysis. One dimensional energy budget did not balance due to large error of the latent heat flux through the surface observation and advection in this area. The large error of the measurement on latent heat flux may depend on the accuracy of the turbulence measurement sensors (Ma et al., 1999b; Ishikawa et al., 1999;
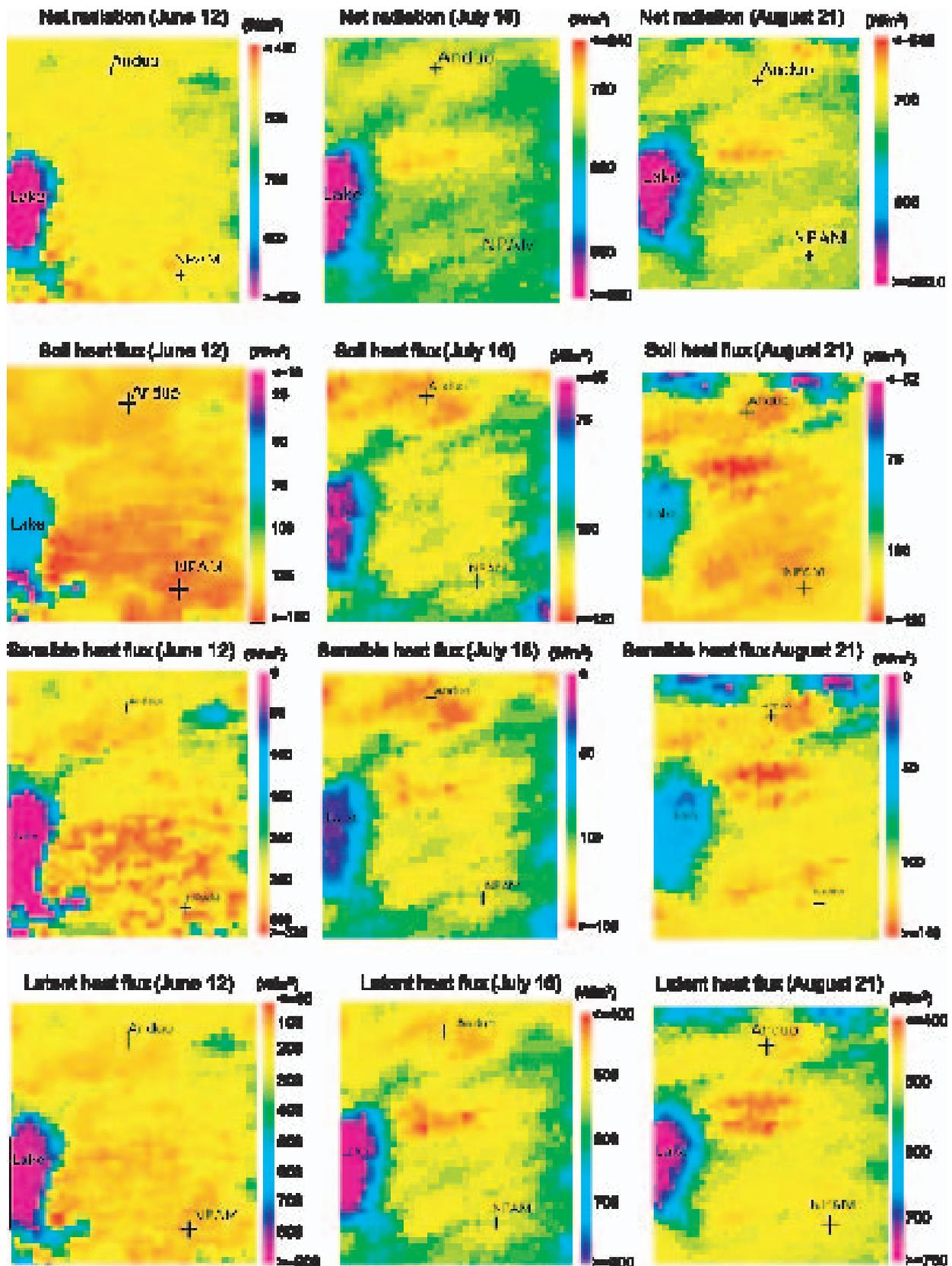
Fig. 6. The distribution maps of land surface heat fluxes for the GAME/Tibet area
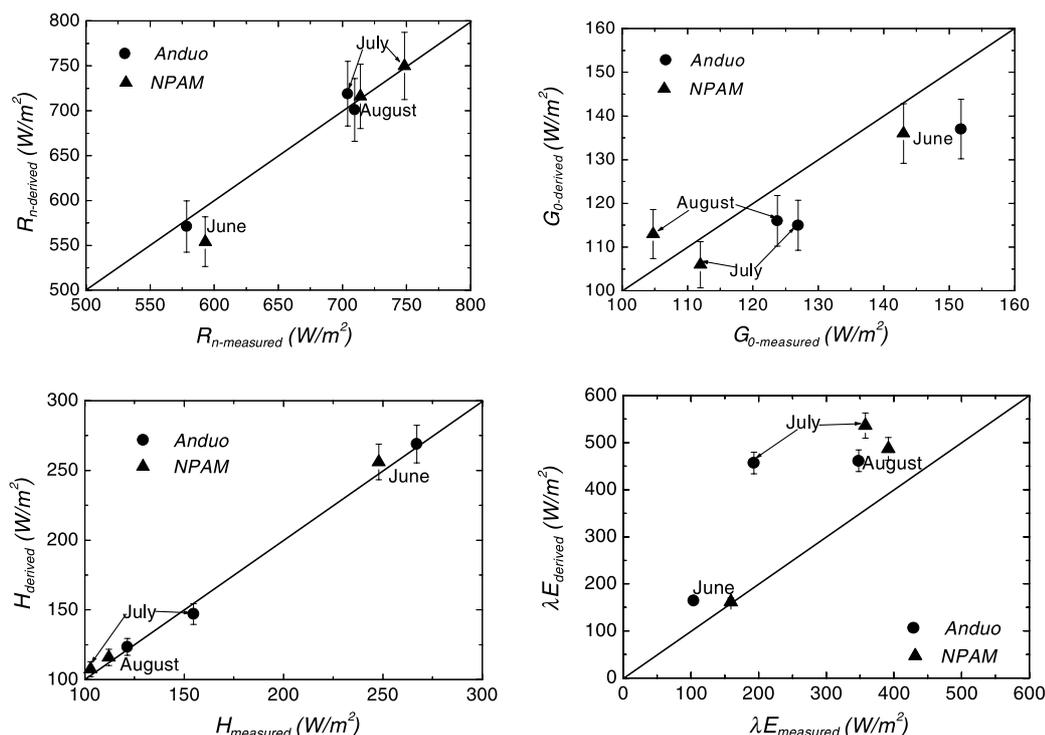
Fig. 7. Comparison of the derived results with the field measurements for the land surface heat fluxes over the GAME/Tibet area, together with 1:1 line

Ma et al., 1999c; Ma et al., 2000; Tanaka et al., 2001). This point and conclusion (a) clearly show the disagreement of latent heat flux between surface observations and satellite one.

4. Concluding remarks

In this paper, the field experiments of the GAME/Tibet and the CAMP/Tibet are introduced and some results on the local surface energy partitioning (diurnal variation, inter-monthly variation and vertical variation etc.) are presented by using the field observational data. The surface energy budget was not well closed from the observed data. The reason for this "imbalance" is pointed out, but further systematic research is necessary to figure out the cause of surface flux imbalances.

The regional distributions and inter-monthly variations of land surface heat fluxes (net radiation, soil heat flux and sensible heat flux) over heterogeneous area of the GAME/Tibet are derived by using NOAA-14/AVHRR data and field observations. The results are in good agreement with field observations. The approach of deriving regional latent heat flux as the residual

of the energy budget may not be a good method due to the measured "imbalance" of energy and the strong advection over the study area. Future improvements are to be made to derive more accurate regional latent heat flux over such areas. It is also worth trying SEBS (Su, 2002) to derived regional land surface heat fluxes, especially for latent heat flux.

All the results in this paper are gotten from high elevation area, the Tibetan Plateau. In order to extend them and the parameterization method presented here to a broader perspective, the results gotten in the Tibetan Plateau have to be compared to them over similar landscape types, i.e. arctic, sub-arctic and alpine etc., and our parameterization method should also be used to the similar landscape types. All these research will be done in the coming days.

References

Bastiaanssen WGM (1995) Regionalization of surface fluxes and moisture indicators in composite terrain. PhD Thesis. Wageningen Agricultural University, 273 pp

Batchvarova E, Gryning SE, Hasager CB (2001) Regional fluxes of momentum and heat over a sub-artic landscape during late winter. Bound-Layer Meteor 99: 489–507

Berk A, Bernstein LS, Robertson DC (1989) MODTRAN, A moderate resolution model for LOTRAN 7, GL-TR-89-0122.

Chen JY, Wang JM, Mitsuta Y (1993) An independent method to determine the surface roughness length. Chinese J Atmos Sci 17(1): 21–26

Chodhury BJ, Idso SB, Reginato RJ (1987) Analysis of an empirical model for soil heat flux under a growing wheat crop for estimating evaporation by infrared-temperature based energy balance equation. Agric Forest Meteorol 39: 283–297

Chodhury BJ, Monteith JL (1988) A four-layer model for the heat budget of homogeneous land surfaces. Quart J Roy Meteor Soc 114: 373–398

Clothier BE, Clawson KL, Pinter PJ, Moran MS, Reginato RJ, Jackson RD (1986) Estimating of soil heat flux from net radiation during the growth of alfalfa. Agric Forest Meteorol 37: 319–329

Daughtry CST, Kustas WP, Moran MS, Pinter PJ, Jackson RD, Brown PW, Nichols WD, Gay LW (1990) Spectral estimates of net radiation and soil heat flux. Remote Sensing Environ 32: 111–124

Gryning SE, Batchvarova E, de Bruin HAR (2001) Energy balance of sparse coniferous high-latitute forest under winter conditions. Bound-Layer Meteor 99: 465–488

Huete AR, Jackson RD, Post DF (1985) Spectral response of a plant canopy with different soil backgrounds. Remote Sensing Environ 17: 37–53

Huete AR (1989) Soil influences in remotely sensed vegetation-canopy spectra. In: Asrar G (ed) Theory and applications of optical remote sensing. New York, USA: John Wiley & Sons. Inc., pp 107–141

Ishikawa H, Hayashi T, Tanaka K, Tsukamoto O, Fudeyasu H, Tamagawa I, Asanuma J, Miyazaki S, Qi Y, Ma YM, Hu ZY, Gao HC (1999) Summary of the boundary layer observation and the preliminary analysis. Third International Scientific Conference on the Global Energy and Water Cycle, Beijing, China, 16–19 June 1999: 45–46

Kenizys FX, Abreu LW, Anderson GP, Chetwynd JH, Shettle EP, Berk A, Bernstein LS, Robertson DC, Acharya P, Rothman LS, Selby JEA, Gallery WO, Clough SA (1996) In: Abreu LW, Anderson GP (eds) The MODTRAN3/2 report and LODTRAN 7 Model prepared by Ontar Corp., North Andover, MA, for Phillips Laboratory, Geophysical Directorate, Hanscom AFB, MA., Contract No. F19628-91-C-0132.

Kustas WP, Daughtry CST (1990) Estimation of the soil heat flux/net radiation ratio from spectral data. Agric Forest Meteorol 39: 205–223

Li ZL, Becker F (1993) Feasibility of land surface temperature and emissivity determination from AVHRR data. Remote Sensing Environ 43: 67–85

Lee XH (1998) On micrometeorological observations of surface-air exchange over tall vegetation. Agric Forest Meteorol 91: 39–49

Lhomme JP, Chehbouni A, Monteny B (1994) Effective parameters of surface energy balance in heterogeneous landscape. Bound-Layer Meteor 71(3): 297–310

Ma YM, Wang JM, Menenti M, Bastiaanssen WGM (1999a) Estimation of fluxes over the heterogeneous land surface with the aid of satellite remote sensing and field observation. ACTA Meteor Sinica 57: 180–189

Ma YM, Tsukamoto O, Wang JM, Ishikawa H, Hu ZY, Tamagawa I, Gao HC (1999b) The characteristics of micrometeorology in the northern Tibetan Plateau area. Proceedings of the 1st International Workshop on GAME-Tibet, Xi'an, China, 11–13 January 1999: 99–102

Ma YM, Tsukamoto O, Wang JM, Hu ZY, Ishikawa H, Tamagawa I, Gao HC (1999c) Transfer and micrometeorological characteristics in the surface layer of the atmosphere above Tibetan Plateau area. Third International Scientific Conference on the Global Energy and Water Cycle, Beijing, China, 16–19 June 1999: 55–56

Ma YM, Tsukamoto O, Wu XM, Tamagawa I, Wang JM, Ishikawa H, Hu ZY, Gao HC (2000) Characteristics of energy transfer and micrometeorology in the surface layer of the atmosphere above marshland of the Tibetan Plateau area. Chinese J Atmos Sci 24(5): 715–722

Ma YM, Tsukamoto O, Wang JM, Ishikawa H, Tamagawa I (2002a) Analysis of aerodynamic and thermodynamic parameters over the grassy marshland surface of Tibetan Plateau. Progress in Natural Sci 12(1): 36–40

Ma YM, Tsukamoto O (2002b) Combining satellite remote sensing with field observations for land surface heat fluxes over inhomogeneous landscape. Beijing, China: China Meteorological Press

Ma YM, Tsukamoto O, Ishikawa H, Su ZB, Menenti M, Wang JM, Wen J (2002c) Determination of Regional land surface heat flux densities over heterogeneous landscape of HEIFE integrating satellite remote sensing with field observations. J Meteor Soc Japan 80(3): 485–501

Mason P (1988) The formation of areally averaged roughness lengths. Quart J Roy Meteor Soc 114: 399–420

Menenti M, Bastiaanssen WGM, Hefny K, Abd EI Karim MH (1991) Mapping of ground water losses by evapora-

tion in the Western Desert of Egypt. DLO Winand Staring Centre, Report no. 43. Wageningen, The Netherlands: 116 pp

Paltridge W, Mitchell RM (1990) Atmospheric and viewing angle correction of vegetation indices and grassland fuel moisture content derived from NOAA/AVHRR. Remote Sensing Environ 31: 121–135

Paulson CA (1970) The mathematic representation of wind speed and temperature profiles in the unstable atmospheric surface layer. J Meteor Soc Japan 9: 856–861

Qi JG, Chehbouni A, Huete AR, Kerr YH, Sorooshian S, (1994) A modified soil adjusted vegetation index. Remote Sensing Environ 48: 119–126

Raupach MR (1994) Simplified expressions for vegetation roughness length and zero-plane displacements as functions of canopy height and area index. Bound-Layer Meteor 71: 211–216

Sobrino JA, Raissouni N (2000) Toward remote sensing methods for land cover dynamic monitoring: application to Morocco. Int J Remote Sensing 21(2): 353–366

Su ZB (2002) The Surface Energy Balance System (SEBS) for estimation of turbulent heat fluxes. Hydrology and Earth System Sciences 6(1): 85–99

Tanaka K, Ishikawa H, Tamagawa I, Ma YM (2001) Surface energy budget at Amdo on Tibetan Plateau using GAME/Tibet IOP'98 data. J Meteor Soc Japan 79(1B): 505–517

Taylor PA, Sykes RI, Mason PJ (1989) On the parameterization of drag over small scale topography in neutrally stratified Boundary flow. Bound-Layer Meteor 48: 409–422

Valiente JA, Nunez M, Lopez-Baeza E, Moreno JF (1995) Narrow-band to broad-band conversion for Meteosatvisible channel and broad-band reflectance using both AVHRR-1 and -2 channels. Int J Remote Sensing 16(6): 1147–1166

Valor E, Caselles V (1996) Mapping land surface emissivity from NDVI: application to European, African, and South American areas. Remote Sensing Environ 57: 167–184

Wang JM, Ma YM, Menenti M, Bastiaanssen WGM (1995) The scaling-up of processes in the heterogeneous landscape of HEIFE with the aid of satellite remote sensing. J Meteor Soc Japan 73(6): 1235–1244

Webb EK (1970) Profile relationships: the log-liner range and extension to strong stability. Quart J Roy Meteor Soc 96: 67–90

Yanai M, Li CY, Song Z (1992) Seasonal heating of the Tibetan Plateau and its effects on the evolution of the Asian summer monsoon. J Meteor Soc Japan 70: 319–351

Ye DZ, Gao YX (1979) The Meteorology of the Qinghai-Xizang (Tibet) Plateau. Beijing: Science Press, 278 pp

Ye DZ (1981) Some characteristics of the summer circulation over the Qinghai-Xizang(Tibet) Plateau and its neighborhood. Bull Amer Meteor Soc 62: 14–19

Ye DZ, Wu GX (1998) The role of the heat source of the Tibetan Plateau in the General circulation. Meteorol Atmos Phys 67: 181–198

Zhang QJ, Zhu BZ, Zhu FK, Weng D, Sun G, Lu J, Peng Y, Wang Y (1988) Advances in the Qinghai-Xizang Plateau Meteorology. The Qinghai-Xizang Plateau Meteorological Experiment (1979) and Research. Science Press, 268 pp

Authors' addresses: Prof. Yaoming Ma (e-mail: ymma@itpcas.ac.cn), and Prof. Tandong Yao, Institute of Tibetan Plateau Research, Chinese Academy of Sciences, Beijing 100085, China; Prof. Hongchao Zuo and Prof. Zeyong Hu, Cold and Arid Regions Environmental and Engineering Research Institute, Chinese Academy of Sciences, Lanzhou 730000, China; Prof. Sanhong Fan, College of Life Science and Technique, Shanxi University, Taiyuan 030006, China; Prof. Hirohiko Ishikawa, Disaster Prevention Research Institute, Kyoto University, Kyoto 611-0011, Japan; Prof. Toshio Koike, Department of Civil Engineering, University of Tokyo, Tokyo 113-8656, Japan; Dr. Zhongbo Su, Alterra Green World Research, Wageningen University and Research Centre, Wageningen 6700AA, The Netherlands.